Case Studies in Engineering Failure Analysis 7 (2016) 56–64

Contents lists available at ScienceDirect

Case Studies in Engineering Failure Analysis

journal homepage: www.elsevier.com/locate/csefa

Case study

Damage analysis of choke bean used in an oil–gas well

H.M. Tawancy *, Luai M. Alhems

Center for Engineering Research, Research Institute, King Fahd University of Petroleum and Minerals, KFUPM Box 1639, Dhahran 31261, Saudi Arabia

ARTICLE INFO

Article history:
Received 7 July 2016
Received in revised form 27 July 2016
Accepted 4 August 2016
Available online 11 August 2016

Keywords:
Oil and gas
Steel
Corrosion
Wear
Electron microscopy

ABSTRACT

A choke bean used in an oil–gas field has catastrophically failed during operation. It is shown that that the damage has been caused by leakage of the corrosive and abrasive drilling fluid. The choke bean adapter made of carbon steel has been corroded and embrittled by hydrogen ingress leading to its fracture in the presence of stresses created by the pressure of accumulated fluid at the bottom section. On the other hand, the choke corner body made of stainless steel has been damaged by abrasive wear of its outer surface.

1. Introduction

Process equipment used in the oil–gas industry relies heavily on various grades of carbon steels and stainless steels as structural materials for several components such as pipes, valves and chokes [1]. An assembly containing such components in addition to spools and fittings is commonly referred to as "Christmas tree" whose primary function is to control the fluid flow into or out of the well by means of chokes, gauges and lines usually referred to as choke manifold. The choke is an orifice installed in the assembly in order to restrict the fluid flow and control the production rate and also create downstream or back pressure [2]. During drilling, a fluid known as the drilling fluid (liquid-based mud) or drilling mud containing additives such as barium sulfate is circulated through the system to remove rock cuttings and bring them to the surface. Another important function of the choke is to control the backflow of the drilling fluid.

Chokes used in oil–gas wells are classified into two major types depending upon the operation mode, which can either be adjustable or positive. Adjustable chokes are flexible in that they allow the fluid flow and pressure to be adjusted in accordance with production requirements. In contrast, positive chokes do not provide that flexibility; however, they are more resistant to damage by abrasion or erosion. Adjustable chokes are usually used in large wells while positive chokes are commonly used in small wells. The calibrated opening of the adjustable choke is usually varied in 0.4 mm (1/64 in.) increments known as beans. Since highly abrasive materials pass through the choke at high speed over several years of service, hardened steel or a grade of stainless steel lined with tungsten carbide is used in the application and a grade of carbon steel is used to manufacture the bean adapter.

During operation, the chokes among other components of the Christmas tree can become susceptible to degradation by various types of wear [3–9], corrosion [1,5,10] and environmental-assisted cracking [11–13]. Although the terms Christmas

* Corresponding author. Fax: +966 13 8603996.
E-mail address: tawancy@kfupm.edu.sa (H.M. Tawancy).

http://dx.doi.org/10.1016/j.csefa.2016.08.001

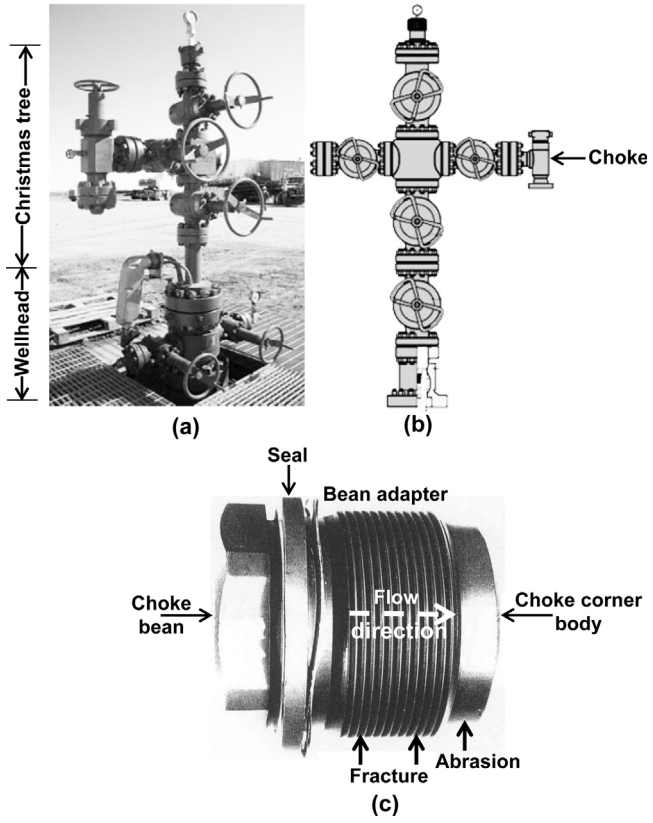

Fig. 1. An illustration of the layout of Christmas tree and wellhead showing the coke used to control the production rate and backflow of the drilling fluid. (a) A photograph showing the Christmas tree and wellhead used in oil–gas wells [2]. (b) A schematic illustration of the Christmas tree showing the location of the choke [2]. (c) A photograph of unused choke in the present study showing its components and the locations of the damage sustained during operation.

tree and wellhead are sometimes used interchangeably, the terms refer to separate equipment as illustrated in the photograph of Fig. 1a [2]. A schematic illustrating the Christmas tree showing the location of the choke is shown in Fig. 1b [2].

In the present case, an adjustable choke bean has been used in service at intermittent periods in an oil–gas well. During the last operation, the choke bean has catastrophically failed within the first hour of operation. The components of a choke bean never used in service are shown in the photograph of Fig. 1c. On-site inspection has shown two types of damage at the bottom of the choke as illustrated in Fig. 1c: (i) the choke bean adapter has fractured along the longitudinal direction, which is parallel to the flow direction and (ii) the outer surface of the choke corner body has sustained severe abrasive wear near the bean adapter. According specifications, AISI 1045 carbon steel and 316L stainless steels have been used to manufacture the choke bean adapter and the choke corner body respectively. The internal surface of the choke corner body has been protected by a surface layer of tungsten carbide. A water-based mud has been used as the drilling fluid. The base is an aqueous solution of Ca and Zn bromides and the solids consist of: (i) clays, (ii) organic colloids, (iii) barium sulfate to increase the fluid density and (iv) substances from the formation (region of the oil–gas reservoir) which are incorporated into the mud during drilling [14]. Items received to determine the most probable cause of failure included the failed choke components, a sample of the drilling fluid and as well as a solid mud sample.

2. Experimental procedure

Representative metallographic specimens were removed from the damaged and unused bean adapters for metallurgical evaluation using scanning electron microscopy (SEM) combined with microchemical analysis by energy dispersive spectroscopy (EDS). The chemical compositions of the choke bean adapter and choke corner body were determined by inductively coupled plasma-atomic emission spectroscopy (ICP-AES) with the exception of C content, which has been measured by combustion calorimetry. To reveal the grain structures, selected specimens were etched in 10% oxalic acid. Surface hardness measurement was used to evaluate the mechanical strength. Since the surfaces exposed by failure of the choke bean adapter were oxidized, selected specimens were descaled in hydrochloric acid to reveal the underlying morphological features. X-ray fluorescence was used to determine the average composition of the drilling fluid. The solid mud sample was analyzed by SEM and EDS.

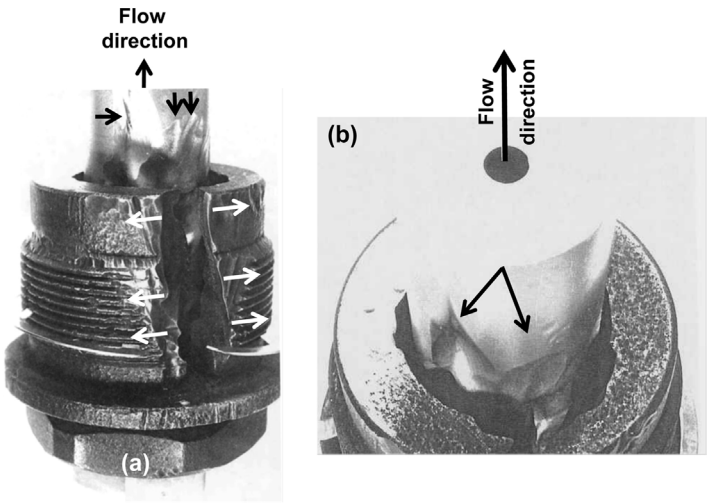

Fig. 2. Photographs illustrating the damage sustained by the choke. (a) Longitudinal fracture of the choke bean adapter and abrasive wear of the outer surface of choke corner body. (b) An illustration of the abrasive wear in comparison with the normal passage of the drilling fluid.

3. Experimental results

3.1. Damage sustained by the choke

Since catastrophic failure has been encountered within the first hour of last operation, it is most likely that the damage sustained by the choke has been accumulative and reached the critical stage prior to the incident of failure. Photographs illustrating the respective damage are shown in Fig. 2 as well as the prescribed flow direction of the drilling fluid through the inner protected surface of the choke corner body. As shown in Fig. 2a and b, the outer surface of the choke corner body appears to have sustained severe damage by abrasive wear leading to considerable loss of material. On the other hand, the bean adapter has fractured along the longitudinal direction as shown in Fig. 2a with corrosion product observed at the exposed surfaces.

It is evident from the observations of Fig. 2 that there has been considerable leakage of the drilling fluid bringing it into contact with the wrong surfaces. Evidently, this leakage has led to continuous dripping and accumulation of the corrosive fluid at the bottom section of the choke bean adapter. Simultaneously there has been fluid flow bypassing the internal surface of the choke corner body and coming into contact with the outer surface at high speed. Fig. 2a shows that fracture of the bean adapter has occurred normal to the direction of maximum tensile stress (tangential stress) created by the fluid pressure.

Fig. 3 summarizes the results of analyzing the composition of the drilling fluid by X-ray fluorescence noting that detection is limited to elements with atomic number ≥ 11. The results of quantifying the spectral data are shown in the inset. It is

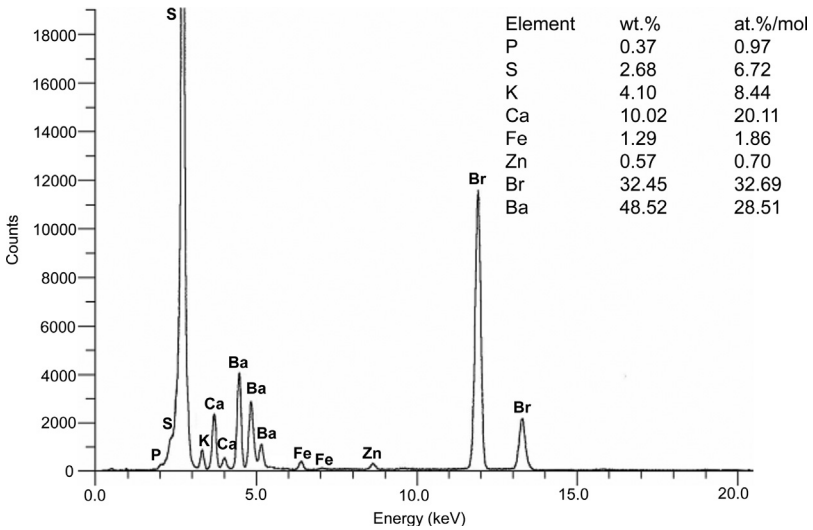

Fig. 3. X-ray fluorescence spectrum showing the elemental composition of the drilling fluid and the results of quantifying the spectral data.

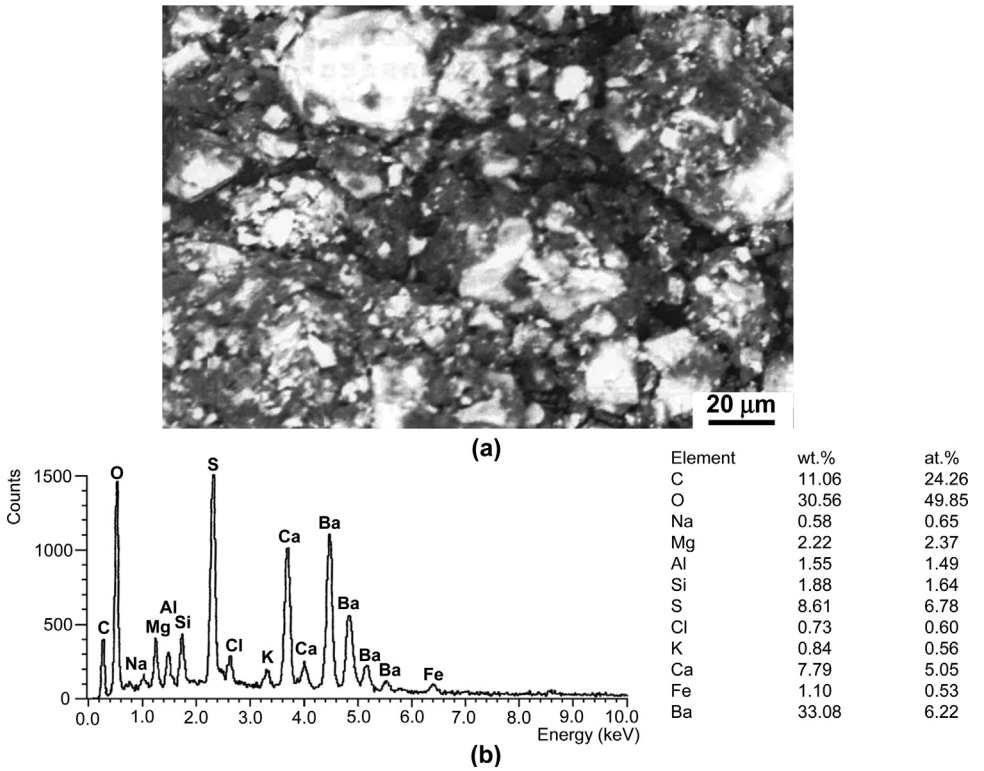

Element	wt.%	at.%
C	11.06	24.26
O	30.56	49.85
Na	0.58	0.65
Mg	2.22	2.37
Al	1.55	1.49
Si	1.88	1.64
S	8.61	6.78
Cl	0.73	0.60
K	0.84	0.56
Ca	7.79	5.05
Fe	1.10	0.53
Ba	33.08	6.22

Fig. 4. Analysis of solid mud sample using SEM and EDS. (a) Secondary electron SEM image illustrating the mud morphology. (b) Corresponding EDS spectrum illustrating the elemental composition and the results of quantifying the spectral data.

observed that the major elemental constituents are Ba and Br with smaller concentrations of Ca, K, S and Fe, and minor concentrations of P and Zn. Fig. 4a is a secondary electron SEM image showing the morphology of the mud sample. The corresponding EDS spectrum and results of quantifying the spectral data are shown in Fig. 4b. As can be seen, Ba, O and C are the major elemental constituents with smaller concentrations of S and Ca, Mg, Si, Al and Fe, and minor concentrations of K and Na. It is possible to conclude from the data of Figs. 3 and 4 that the water-based mud of the drilling fluid has likely contained some dissolved CO_2 and H_2S as confirmed later by the results of analyzing the corrosion product deposited at the inner surface of the choke bean adapter.

To summarize, the above observations indicate that the failure has occurred due to leakage of highly abrasive and corrosive fluid bring it into direct contact with the wrong surfaces (inner surface of the choke bean adapter and outer surface of the choke corner body). This is further supported by the detailed microstructural characterization presented later.

3.2. Characterization of unused choke

Typical microstructures of unused sections of AISI 1045 carbon steel and 316L stainless steel used in the choke application are shown in Figs. 5 and 6 respectively. Fig. 5 shows the microstructure of AISI 1045 carbon steel (choke bean adapter) consisting of a mixture of ferrite and pearlite, and corresponding EDS spectrum illustrating its elemental composition. Typical of 316L stainless, its microstructure consists of equiaxed grains with high density of annealing twins as shown in Fig. 6 with elemental composition shown in the corresponding EDS spectrum.

Table 1 summarizes the results of chemical analysis of each steel in comparison with the respective nominal compositions. It is observed that the measured compositions fall within those specified for both steels, which are commonly used in such applications [2].

3.3. Analysis of the fractured bean adapter

A secondary electron SEM image illustrating the gross morphology of the surface exposed by fracture of the bean adapter in the as received condition is Fig. 7a. The corresponding EDS spectrum of Fig. 7b shows that Fe and O and C and S are the major elemental constituents of the surface scale with smaller concentrations of Ca and minor concentrations of Na, Mg, Al, Si, P, K and Mn suggesting that iron carbonate ($FeCO_3$) is the major component of the scale with smaller amount of iron

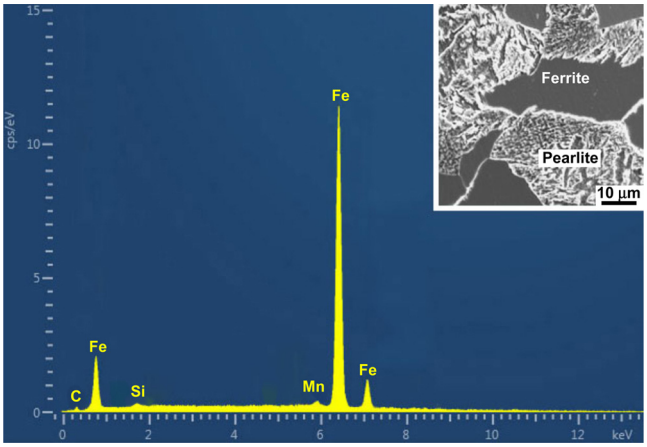

Fig. 5. EDS spectrum and corresponding microstructure of a specimen removed from a section of choke bean adapter never used in service (AISI 1045 carbon steel).

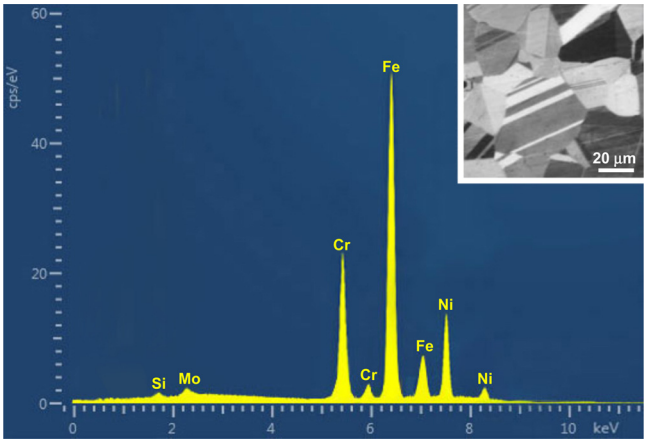

Fig. 6. EDS spectrum and corresponding microstructure of a specimen removed from a choke corner body never used in service (316L stainless steel).

Table 1
Chemical compositions of the steels used in the application (wt%).

ISI1045 carbon steel			316L stainless steel		
	Nominal	Measured		Nominal	Measured
Fe	Balance	98.58	Fe	Balance	66.78
Mn	0.6–0.9	0.68	Cr	16–18	17.20
C	0.43–0.50	0.46	Ni	10–14	11.93
Si	0.15–0.30	0.22	Mo	2–3	2.14
S	0.05[a]	0.03	Mn	2[a]	1.12
P	0.04[a]	0.03	Si	1[a]	0.75
			C	0.03[a]	0.02
			P	0.045[a]	0.03
			S	0.04[a]	0.03

[a] Maximum.

sulfide (FeS) With the exception of Mn, which is present in the steel, Ca and other minor elements could have been incorporated into the scale from the drilling fluid.

Deposition of both iron carbonate and iron sulfide at the surface of carbon steel as suggested by the spectral data of Fig. 7b is shown to be possible in acidic solutions due to the presence of aqueous solutions of CO_2 and H_2S in oil–gas wells [15,16]. Formation of the two phases occurs according to the following reactions [15]:

$$Fe + H_2CO_3 \rightarrow FeCO_3 + H_2$$

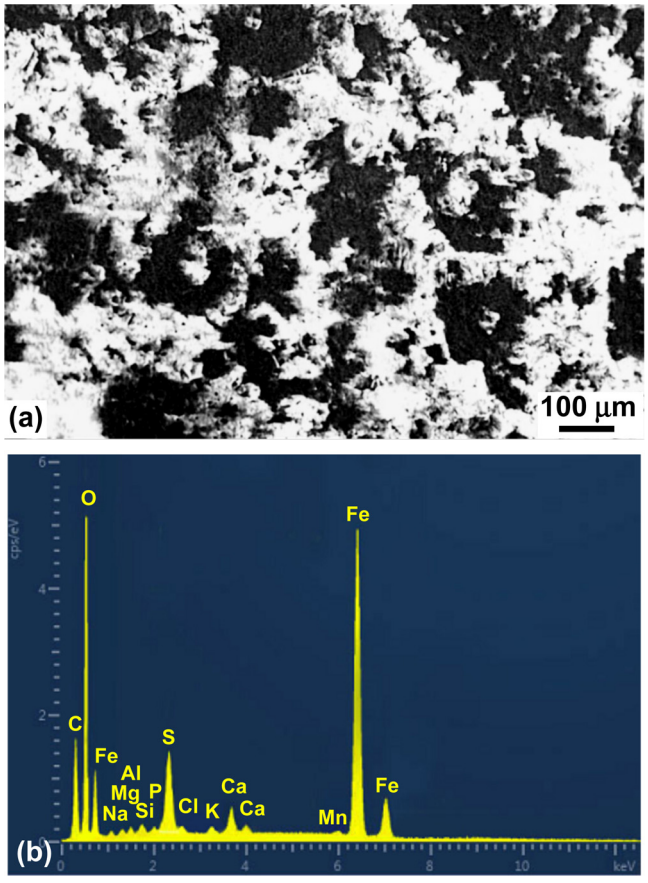

Fig. 7. Analysis of the corrosion deposit observed at the internal surface of the bean adapter near the fracture surface. (a) Secondary electron SEM image illustrating the gross morphology of the corrosion product. (b) Corresponding EDS spectrum illustrating the elemental composition.

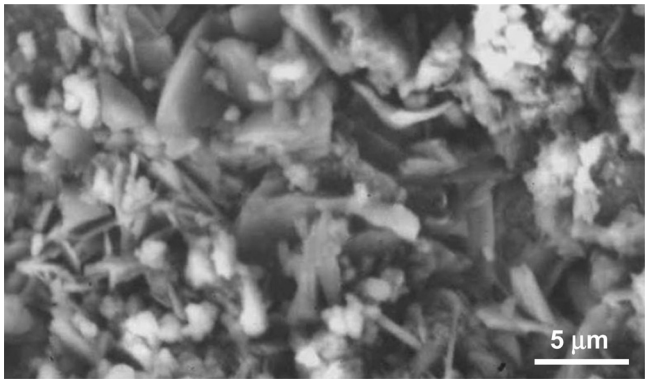

Fig. 8. Morphology of the corrosion deposit in Fig. 7a as viewed at higher magnification.

$$Fe + H_2S \rightarrow FeS + 2H$$

The morphology of the scale shown in Fig. 7a as viewed at higher magnification is shown in Fig. 8.

An example illustrating characteristic macroscopic features of the surface exposed by fracture of the choke bean adapter after descaling is shown in Fig. 9. Voids scattered throughout the surface and small secondary cracks are observed as indicated by the arrows. Fig. 10 shows the morphology of the fracture surface in comparison with the microstructure of a sound section of the steel as viewed at the same magnification. A one-to-one correspondence appears to exist between the two images in Fig. 10 suggesting that fracture has occurred intergranularly particularly near the pearlite colonies. On the other hand, the average surface hardness in the vicinity of the major crack is found to be R_b 86, which is comparable to that of

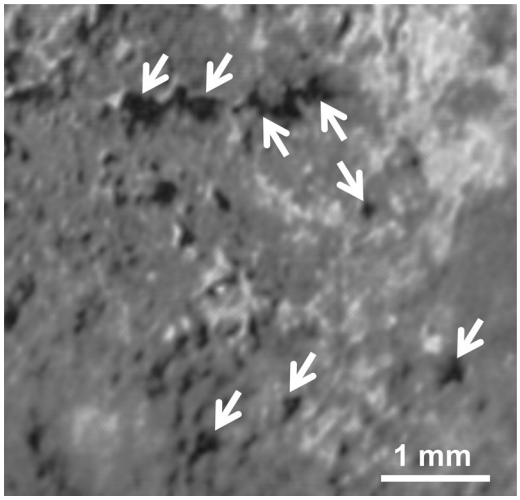

Fig. 9. Secondary electron SEM image illustrating the macroscopic morphology of the surface exposed by fracture of the choke bean adapter after descaling, voids and secondary cracks are indicated by the arrows.

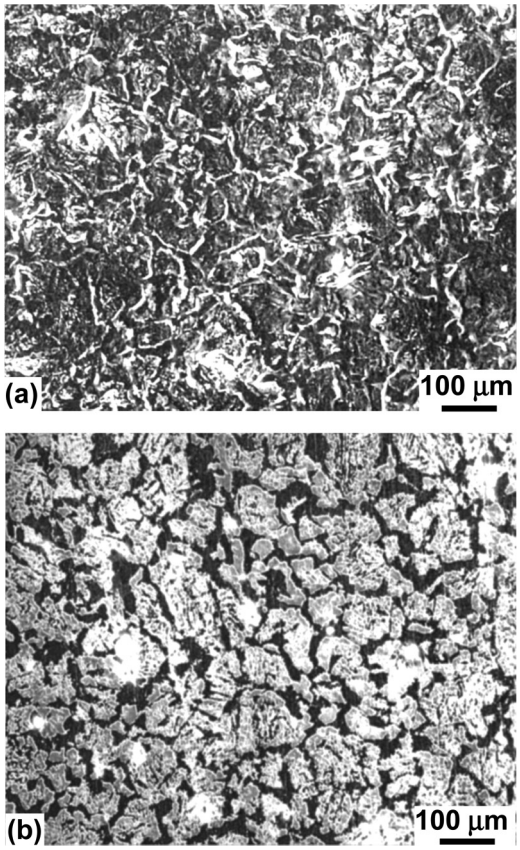

Fig. 10. Secondary electron SEM images illustrating the morphology of fracture surface of the choke bean adapter (a) in comparison with the grain structure of the bean adapter as revealed by polishing and etching (b).

the steel never used in service (R_b 84–87) indicating that the fracture is not related to a hardening effect. Instead, most evidence points out that it is related to hydrogen embrittlement as discussed below.

In the absence of catalyst, when elemental hydrogen released by the above reaction forming FeS comes into contact with the steel surface, it tends to form harmless surface bubbles, however, the presence of elemental S facilitates hydrogen absorption by deterring the formation of bubbles [17]. Dissolved elemental hydrogen tends to segregate at defects such as

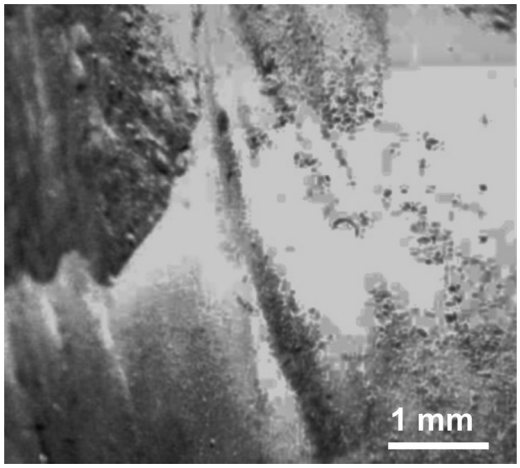

Fig. 11. Secondary electron SEM image illustrating the macroscopic morphology of the outer surface of the choke corner body.

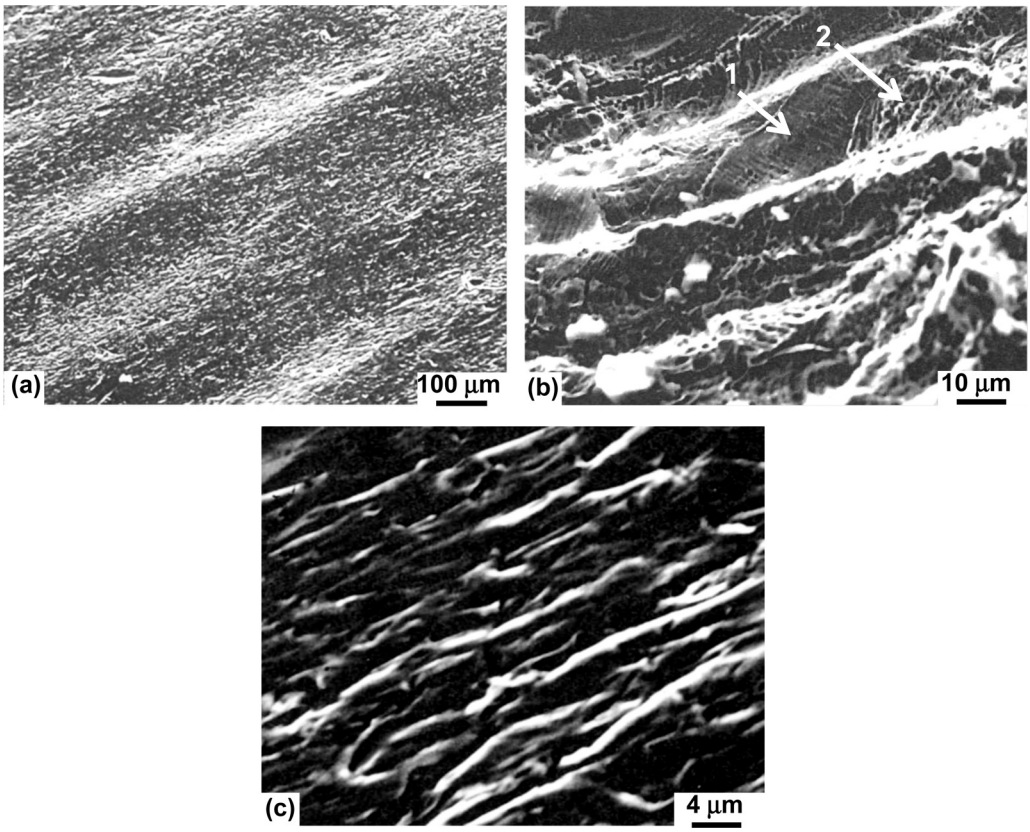

Fig. 12. Secondary electron SEM images illustrating the morphological details of the outer surface of the choke corner body. (a) Gross morphology of grooves created by plowing. (b) Fine striations resembling slip traces (region 1) and region with morphology characteristic of dimple-type rupture (region 2) observed in a groove. (c) Closely spaced ridges observed at higher magnification.

grain boundaries, twin boundaries and dislocations. Continued absorption of elemental hydrogen, can eventually lead to precipitation of molecular gaseous hydrogen (H_2) at internal interfaces. This precipitation is relaxed by formation of internal voids and cracks, which can cause severe embrittlement [17,18]. It is well known that the resistance of steels to hydrogen embrittlement is dependent upon the exact microstructure with the lowest resistance exhibited by pearlitic-type such as that used in the present application [17,19,20]. It is likely, however, that the intergranular effect near the pearlitic colonies results from their preferential anodic dissolution.

3.4. Analysis of the damaged choke corner body

Fig. 11 is a secondary electron SEM image showing the macroscopic morphology of the outer surface of the choke corner body. The morphology is characteristic of that produced by abrasive wear of stainless steels [21]. Abrasive wear is known to involve three mechanisms: (i) plowing, (ii) cutting and (iii) fragmentation [21,22]. Plowing usually occurs by the formation of plastically deformed grooves [23,24] such as those shown in Fig. 12a. Closer examination of the grooves at higher magnification reveals the presence of two characteristic features as shown in Fig. 12b: (i) fine striations (region 1) resembling slip traces and (ii) dimple-type rupture morphology (region 2) resembling that of fracture produced by microvoid coalescence. Furthermore, fine closely-spaced ridges are also observed within the grooves as shown in Fig. 12c, which can be related to removal of material in the form of chips leaving behind ridges at the metal surface [25].

4. Conclusion

It is concluded from the present study that the components of the choke have been damaged by leakage of the abrasive and corrosive drilling fluid. Most evidence point out that the beam adapter has been damaged by corrosion and hydrogen embrittlement in the presence of the stresses created by the fluid pressure eventually leading its fracture along the longitudinal direction. On the other had, the abrasive fluid traveling at high speed and bypassing the normal passage through the internal surface of the choke corner body has lead to abrasive wear of the outer unprotected surface.

Acknowledgements

The authors are grateful for the continued support provided by King Fahd University of Petroleum and Minerals.

References

[1] Albdiry MT, Almensory MF. Failure analysis of drillstring in petroleum industry: a review. Eng. Fail. Anal. 2016;65:74–85.
[2] Devold H. Oil and gas production handbook: an introduction to oil and gas production, transport, refining and petrochemical industry. ABB (ASEA Brown Boveri) Oslo; 2013, www.abb.com/oilandgas.
[3] Wong CY, Solnordal C, Swallow A, Wang S, Graham L, Wu J. Predicting the material loss around a hole due to sand erosion. Wear 2012;276–277:1–15.
[4] Navas G, Grigorescu IC. Erosion-corrosion failures in wellhead chokes, Corrosion-2011, NACE Paper No.11247. Houston: NACE International; 2011.
[5] Hu X, Barker R, Neville A, Gnanavelu A. Case study on erosion-corrosion degradation of pipework located on an offshore oil and gas facility. Wear 2011;271:1295–301.
[6] Arefi A, Settari A, Angman P. Analysis and simulation of erosion in drilling tools. Wear 2005;295:263–70.
[7] Nokleberg L, Sontvedt T. Erosion in choke valves-oil and gas industry applications. Wear 1995;186–187:401–12.
[8] Haugen K, Kvernvold O, Ronold AE, Sandberg R. Sand erosion of wear-resistant materials: erosion in choke valves. Wear 1995;186–187:179–88.
[9] Laptev D, Levin S, Livshitz L. Wear-resistant materials for oil and gas machinery. Wear 1993;162–164:957–61.
[10] Islam MD, Farhat ZN. Characterization of the corrosion layer on pipeline steel in sweet environment. J Mater Eng Perform 2015;24:3142–58.
[11] Liu Y, Lian Z, Lin T, Shen Y, Zhang Q. A study of axial cracking failure of drill pipe body. Eng Fail Anal 2016;59:434–43.
[12] Panda B, Sujata M, Madan M, Bhaumik SK. Stress corrosion cracking in 316L stainless steel bellows of a pressure safety valve. Eng Fail Anal 2014;36:379–89.
[13] Moroz MZ. Environmentally assisted cracking of drill pipes in deep drilling oil and natural gas wells. J Mater Eng Perform 2012;21:1061–9.
[14] Caenn R, Darley HCH, Gray GR. Composition and properties of drilling and completion fluids. 6th ed. Waltham, MA: Elsevier Inc.; 2011. p. 1–37.
[15] Popoola LT, Grema AS, Latinwo GK, Gutti B, Balogun AS. Corrosion problems during oil and gas production and its mitigation. Int J Ind Chem 2013;4:35–49.
[16] Choi YS, Nesic S, Ling S. Effect of H2S on the corrosion of carbon steel in acidic solutions. Electrochim Acta 2011;56:1752–60.
[17] Bernstein IM, Thompson AW. Resisting hydrogen embrittlement. In: Tien , Ansell , editors. Alloy and microstructural design. New York: Academic Press; 1976. p. 303–47.
[18] Flanders N, Tennant R, White WE. Observations of relationships between microstructure and hydrogen-induced cracking. In: Blum , French , Middleton , Vander Voort , editors. Microstructural science vol. 15, field metallography, failure analysis and metallography. Materials Park, OH: ASM International; 1987. p. 227–39.
[19] Bernstein IM, Thompson AW. Effect of metallurgical variables on environmental fracture of steels. Int Mater Rev 1976;21:269–87.
[20] Calavre G, Fontaine JC, Galibois A, Krishnadev MR. Hydrogen embrittlement studies of pearlitic microstructures. In: Blum , French , Middleton , Vander Voort , editors. Microstructural science, vol. 15, field metallography, failure analysis and metallography. Materials Park, OH: ASM International; 1987. p. 241–50.
[21] Hokkirigawa K, Kato K. An experimental and theoretical investigation of ploughing, cutting and wedge formation during abrasive wear. Tribol Intern 1988;21:51–7.
[22] Tylczak JH. Abrasive wear. In: ASM Handbook, vol. 18, Friction, Lubrication and Wear Technology; 2002.
[23] Moore MA. A review of two-body abrasive wear. Wear 1974;27:1–17.
[24] Lai HH, Hsieh CC, Lin CM, Wu W. Effect of vanadium content on the microstructure and dry sand abrasive wear of a eutectic Cr-Fe-C hardfacing alloy. Met Mater Int 2016;22:101–7.
[25] Larson-Badse J. Influence of grit diameter and specimen size on wear during sliding abrasion. Wear 1968;12:35–53.